Supplementary Information

Optical Trapping with High Forces Reveals Unexpected Behaviors of Prion Fibrils

Jijun Dong[1], Carlos E. Castro[2], Mary C. Boyce[2], Matthew J. Lang[2, 3, 4, *] and Susan Lindquist[1, 5, *]

[1]Whitehead Institute for Biomedical Research, 9 Cambridge Center, Cambridge, MA 02142

[2]Department of Mechanical Engineering, [3]Department of Biological Engineering, Massachusetts Institute of Technology, 77 Massachusetts Avenue, Cambridge, MA 02139

[4]Current address: Chemical and Biomolecular Engineering, Vanderbilt University, 2301 Vanderbilt Place, Nashville, TN 37235

[5]Howard Hughes Medical Institute and Department of Biology, Massachusetts Institute of Technology, 77 Massachusetts Avenue, Cambridge, MA 02139

*To whom correspondence should be addressed:

Susan Lindquist, Lindquist_admin@wi.mit.edu; Matthew Lang, matt.lang@vanderbilt.edu

Nature Structural & Molecular Biology: doi:10.1038/nsmb.1954

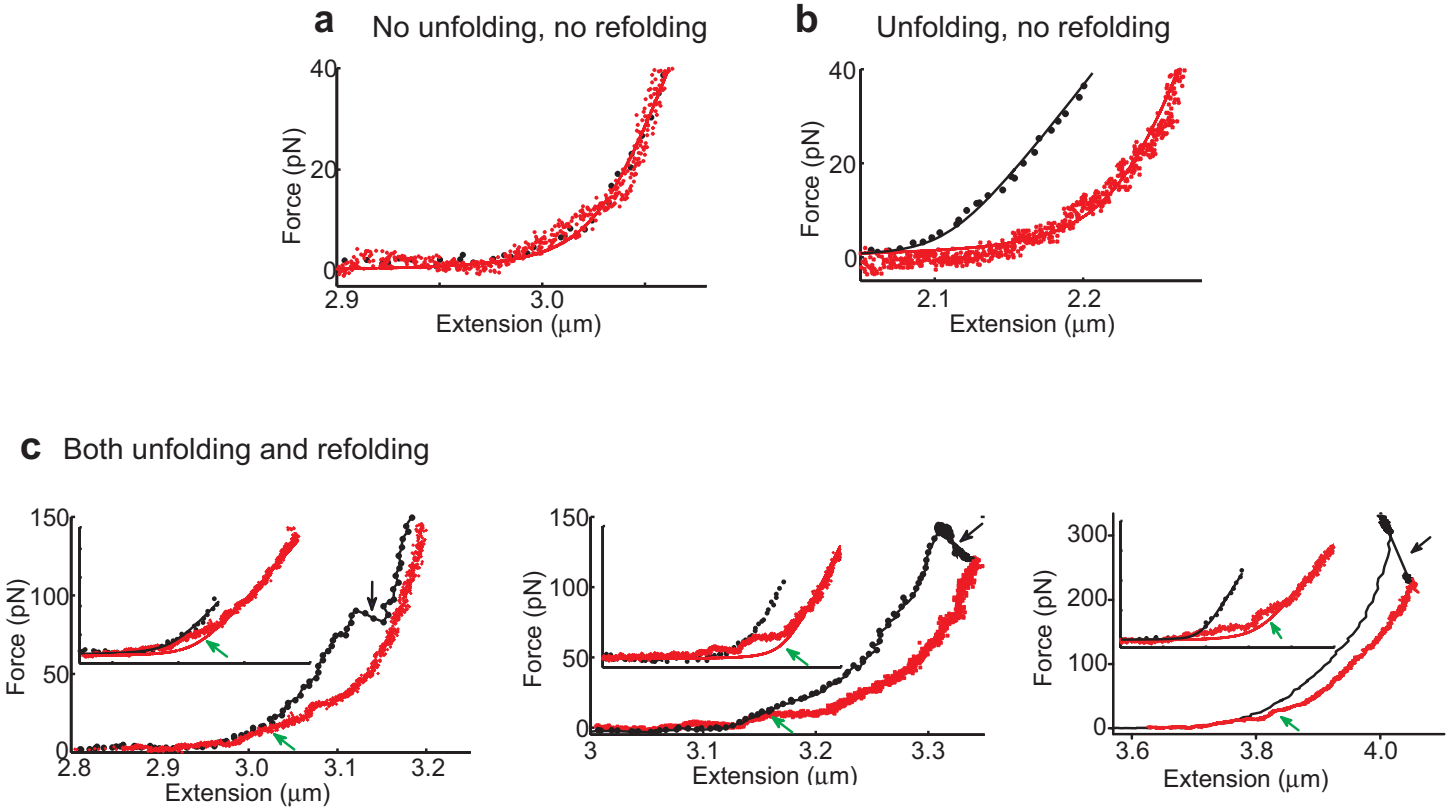

Figure S1 (Lindquist)

Figure S1. Fitting of the force-extension curves of RΔ2-5 fibrils unfolded in physiological buffer suggests that refolding can occur during relaxation at low forces. **(a)** This particular RΔ2-5 fibril did not show any force-dropping events in the stretching curve. As a result, the stretching and relaxation curves were superimposable and can be fit well with the modified WLC model. **(b)** This RΔ2-5 fibril sustained a substantial force-dropping event in the holding phase. As a result, the relaxation curve showed an increase in extension length. The relaxation curve fit well with the modified WLC model, implying no refolding of the fibril. Only the low-force region of both the stretching and relaxation curves were showed in (a) and (b) to magnify the behavior and WLC fitting at low-force region. **(c)** These fibrils, exemplifying the fitted stretching-relaxation cycles obtained with nine out of sixteen RΔ2-5 fibrils, showed evidence of both unfolding and refolding. Force-dropping events were observed in the stretching or/and holding phase. As a result, the relaxation curves showed increases in extension length. In this relaxation phase, curves showed deviations from WLC behavior [4], implying refolding of some unfolded elements in the fibrils.

No suggestion of refolding was observed in the relaxation curves of wild-type prion fibrils. This was not surprising since unfolding was only achieved in the presence of GdHCl and DAPH. As previously shown, these denaturants inhibit prion assembly at much lower concentrations that are required to disassemble the fibrils [5]. Under physiological conditions refolding of RΔ2-5 fibrils was indicated. Unfortunately, we were not able to fully determine the refolding probability by performing multiple stretching-relaxation cycles as typically done for other globular proteins [4,6]. In those experiments, which employ small numbers of well defined protein monomers covalently linked end on end at a single position, the fully unfolded proteins were quickly relaxed to zero extension for a variable period of waiting time before a subsequent stretching curve was measured. Refolding that has occurred during this period is then estimated from unfolding behavior in the next stretching cycle. With prion fibrils, however, the fully unfolded state cannot be reached due to the very larger numbers of monomers in the individual fibrils. Therefore, unfolding behavior in the next stretching cycle can't be simply attributed to the refolding of the same region that unfolded previously. It could represent unfolding of a new previously folded region. Nevertheless, non-identical refolding behaviors among different relaxation curves suggest a complex refolding landscape for RΔ2-5 fibrils.

Nature Structural & Molecular Biology: doi:10.1038/nsmb.1954

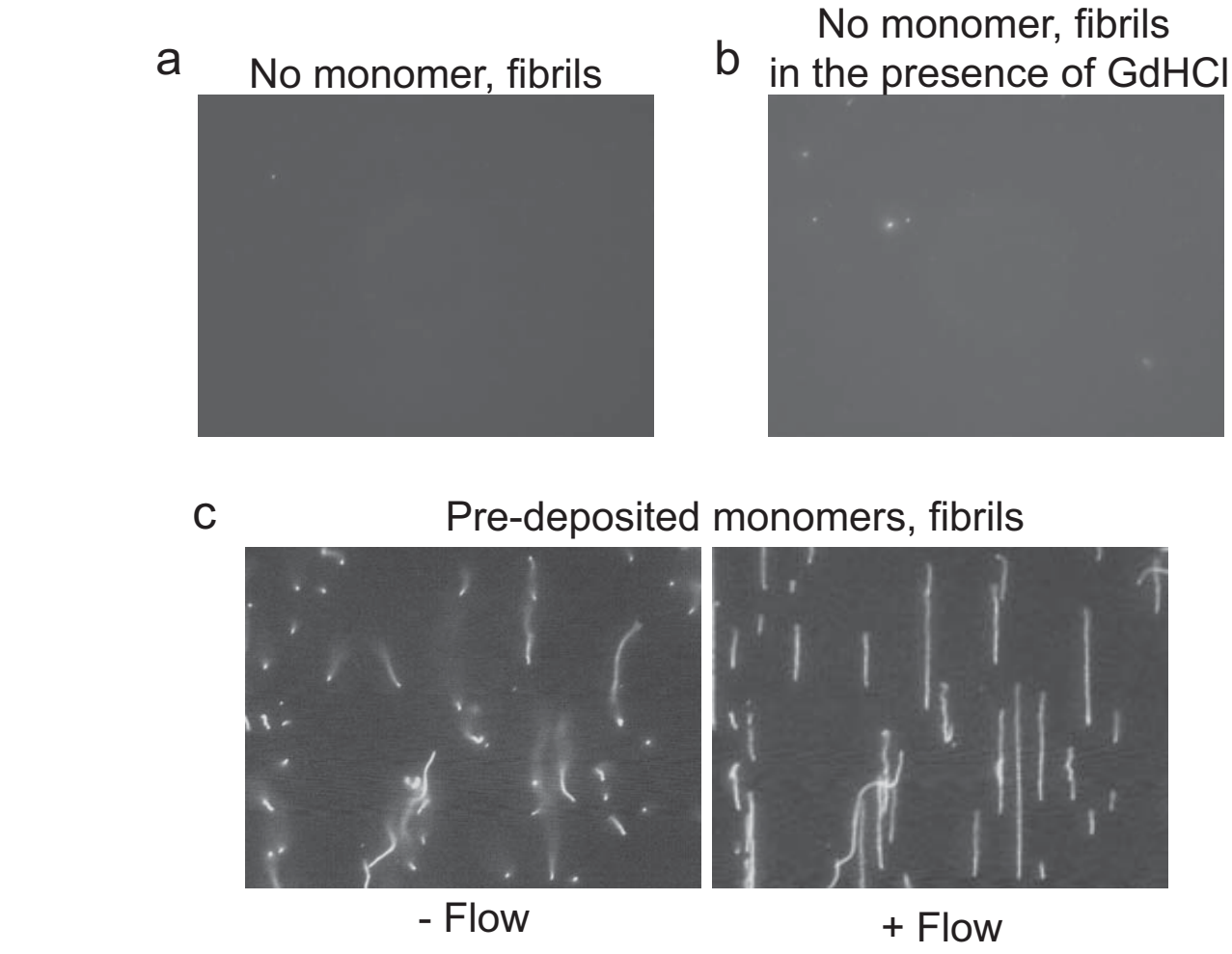

Figure S2 (Lindquist)

Nature Structural & Molecular Biology: doi:10.1038/nsmb.1954

Figure S2. The presence of 1.2 M GdHCl prevented pre-deposited NM monomers from recruiting NM fibrils to the glass surface and very rarely produced any additional points of attachment. **(a)** No NM monomers were pre-deposited. The flow chamber was blocked with casein directly and then incubated with 1μM NM fibrils for 15 min in the presence of assembly buffer. **(b)** No NM monomers were pre-deposited. The flow chamber was blocked with casein directly and then incubated with 1μM NM fibrils for 15 min in the presence of 1.2 M GdHCl. **(c)** NM monomers were pre-deposited. After being blocked with casein, the flow chamber was then incubated with 1μM NM fibrils for 15 min in the presence of assembly buffer. ***Left***, the image was taken without a flow. ***Right***, the same area was imaged with a flow that straightened the fibrils for visualization of the full length of the fibrils in the imaging plane. **(d)** NM monomers were pre-deposited. After being blocked with casein, the flow chamber was then incubated with 1μM NM fibrils for 15 min in the presence of 1.2 M GdHCl. No fibrils were detected in most of the sample areas as shown in two images on the left, while in very rare cases a few fibrils were detected as shown on the right.

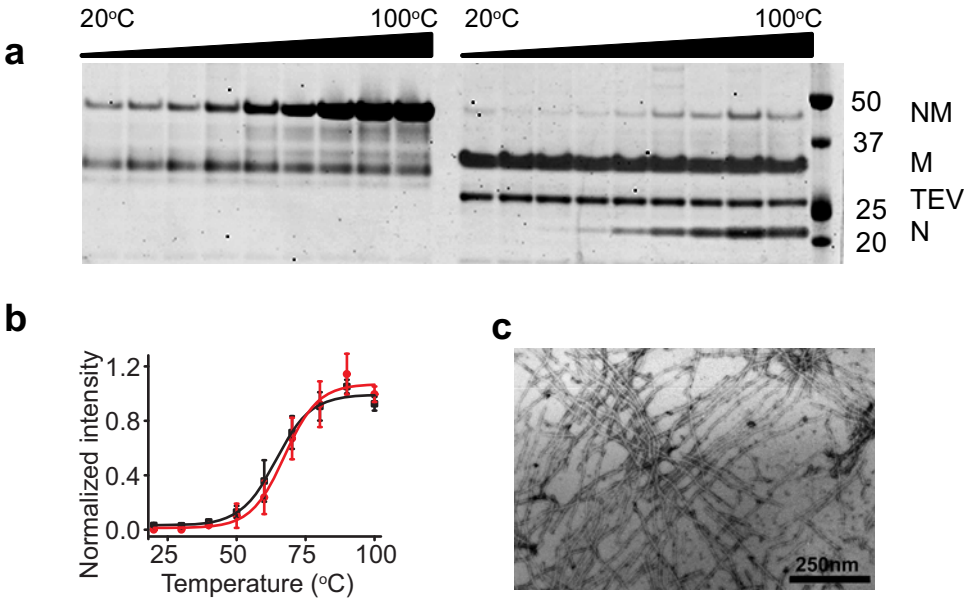

Figure s3 (Lindquist)

Figure S3. The M domain is not involved in the amyloid core of NM fibrils. **(a)** Fibrils formed by NM proteins with a TEV cleavage site at position 142-148 were treated without (*left*) or with (*right*) TEV protease. The stability of the TEV-treated fibrils was determined by treatment under increments of temperature and examined by SDS–PAGE. **(b)** The band intensities, which reflect susceptibility of aggregates to thermal solubilization, were averaged from four independent experiments as shown in (a) and plotted as a function of temperature and fitted to a sigmoidal function. Black, the band intensities of NM monomers in the absence of TEV protease; red, the band intensities of the N fragments after TEV treatment. **(c)** Transmission electron microscope image of NM fibrils after TEV cleavage.

Nature Structural & Molecular Biology: doi:10.1038/nsmb.1954

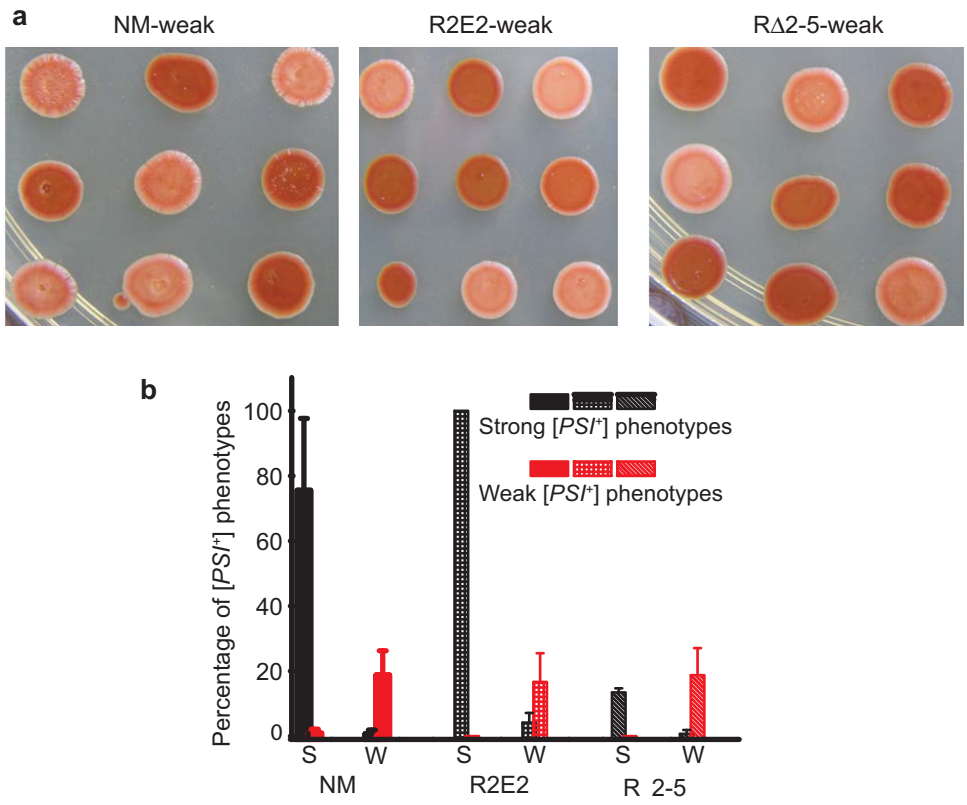

Figure S4 (Lindquist)

Figure S4. Characterization of R2E2 and RΔ2-5 fibrils that carry weak prion elements. **(a)** The prion status of "weak" NM (***left***), R2E2 (***middle***) and RΔ2-5 (***right***) fibrils was confirmed by protein-only transformation. Assembly of soluble NM was seeded by lysates of yeast cells that carried a weak prion element. The reaction was performed at 37°C. The uniform weak prion phenotypes were indicated by the dark salmon color colonies. **(b)** Quantification of transformation efficiency and specificity of distinct prion fibrils. "S" refers to the fibrils seeded at 4°C by cell lysates carrying a strong prion element, while "W" refers to the fibrils seeded by cell lysates at 37°C carrying a weak prion element. For each column, the bar in black shows the percentage of colonies carrying strong prion phenotypes after protein-only transformation, while the bar in red shows the percentage of colonies carrying weak prion phenotypes.

Supplementary methods

Labeling of NM monomers. To label NM monomers with fluorophore or biotin, 100 μM of NM proteins with a single cysteine residue at position 184 were incubated with 2mM Alexa Fluor 555 C2 maleimide (Invitrogen, Carlsbad, CA) or Maleimide-PEO2-Biotin (thermo scientific, Rockford, IL) overnight at 4°C in 10mM Tris buffer in the presence of 6 M GdHCl and 0.5mM TCEP. The labeled proteins were purified using desalting columns and pelleted with 70% methanol. Fibrils were assembled in vitro from a mixture of purified wild-type NM protein and fluorescently labeled NM in 1xCRBB buffer (5 mM potassium phosphate, 150 mM NaCl and 5 mM TCEP). Ten percent-, 25%-, 50%- and 75%-fluorescently labeled NM monomers were tested for optimized fluorescent imaging and 50% of labeling monomers were used in all the experiments.

Protein-only transformation. The prion nature of the preformed fibrils was confirmed by following a previously published protocol for in vitro fibril transformation with slight modifications (*2*). Yeast cells ([*psi*$^-$][*PIN*$^+$] derivative of 74D-694 [MATa, *his3, leu2, trp1, ura3*; suppressible marker *ade1-14*(UGA)]) were grew in YEPD media (1% yeast extract, 2% bactopeptone, 2% dextrose) (typically 50 ml) to an OD_{600} of 0.5 and then successively washed with 20 ml of sterile H_2O, 1 M sorbitol, and ST buffer (1 M sorbitol, 10 mM Tris, pH 7.5). The cells were spheroplasted with lyticase (Sigma-Aldrich, ~200 units for yeast cells cultured from 50 ml YEPD) in ST buffer at 30°C for 30 min. The spheroplasts were then collected by centrifugation (400x*g*, 4 min), successively washed with 5 ml of 1 M sorbitol and STC buffer (1 M sorbitol, 10 mM $CaCl_2$, 10 mM Tris, pH 7.5) and resuspended in 1 ml of STC-buffer. One hundred μl of the yeast spheroplasts were mixed with 25 μl of sonicated amyloid fibrils, *URA3* marked plasmid (pRS316) (20 μg/ml) and salmon sperm DNA (100 μg ml^{-1}). The amyloid fibrils were concentrated by centrifugation of 1 ml of 5 μM reaction solution into 200 μl, giving a concentration of 25 μM. Next, 9 volumes of PEG-buffer (20% [w/v] PEG 8000, 10 mM $CaCl_2$, 10 mM Tris, pH 7.5) were added into the mixture and the reaction was incubated at room temperature for 30 min to induce fusion. Cells were collected by centrifugation (400x*g*, 4 min) and resuspended with 150 μl of SOS-buffer (1 M sorbitol, 7 mM $CaCl_2$, 0.25% yeast extract, 0.5% bacto-peptone), incubate at 30°C for 30 min. The recovered cells were resuspended into 7 ml of synthetic media lacking uracil (20 g L^{-1} Dextrose, 6.7 g L^{-1} Yeast Nitrogen base with no amino acids, 0.75 g L^{-1} CSM-URA amino acid supplement, 20 g L^{-1} agar, 1 M sorbitol) and immediately plated into plates with the same synthetic media. After incubation at 30°C for ~5 days, single colonies randomly chosen from the SD-URA plates were spotted onto YEPD plates containing 1/4 of the standard amount of yeast extract to determine [*PSI*$^+$] and [*psi*$^-$] states.

Preparation of the samples for optical trapping. Experiments were carried out in a flow chamber made of a glass cover slip attached to a glass microscope slide via double-sided sticky tape to create a channel of approximately 10-15 μl in volume. His-tagged NM monomers at a concentration of 0.1 to 0.5 μM were flown into the channel and incubated for 15 min to allow for adsorption to the glass cover slip surface. Five-mg/ml casein (Sigma-Aldrich) was then flown into the channel and incubated for 40 min to cover the remaining exposed cover slip surface and prevent further non-specific interactions with the glass. Pre-formed fluorescently labeled fibrils were flown into the chamber at a concentration of 0.1 to 0.5 μm and incubated for 10 to 20 min.

Free fibrils were washed away with 200 μl of 1xCRBB buffer for three times. NM-coated polystyrene beads (800 nm) were flown into the flow channel and incubated overnight to allow beads to attach to free fibril ends. Slides were washed three times with 200 μl of 1xCRBB buffer containing 0.1 mg ml^{-1} casein before the start of the experiment to remove any free beads from the flow channel. It is very important to freshly prepare and filter every reagent.

To prepare the NM-coated beads, 10 μl of pre-washed streptavidin-coated polystyrene beads (Spherotech, 1% w/v) were mixed with 500 μl of 5 μM biotinylated NM and 0.2 μM of biotinylated Alexa488 fluorescent markers (Invitrogen) in the presence of 1mg/ml casein at room temperature. After a 30-min incubation, the beads were washed and dissolved in 500 μl of 1xCRBB buffer with 5mM TCEP and 0.1% $mg.ml^{-1}$ casein for use.

Cleavage of the M domain after NM proteins assembled into fibrils. NM proteins with a TEV cleavage site at position 143 to 149 were seeded with yeast cell lysates carrying wild-type strong prion elements at 4°C. Once the assembly reactions completed, TEV protease was added into the solutions and each reaction was then divided into nine aliquots. After incubation at 30^{o}C overnight, the aliquots were heated at different temperatures ranging from 20°C to 100°C and then analyzed by SDS-PAGE. The gels were stained with coomassie blue and the band intensities were quantified and normalized to the bend intensity at 100°C.

Stretching of prion fibrils under different experimental conditions. Fibrils were assembled as described above in the normal 1xCRBB buffer and were attached to the glass surface at one end and to the bead at the other end. After the bead was centered and the instrument was calibrated, 1xCRBB buffer containing GdHCl or DAPH was introduced to the flow chamber. Collection of force-extension curves from multiple stretching-relaxation cycles were started and normally finished within 6 h. At the end, unfolding events had become only slightly more frequent, with no noticeable change in the nature of the events.

Determination of the maximum force capacity of our trapping instrument. The force-extension behavior of the NM fibrils was used as an internal control to confirm the maximum force capacity of our trapping instrument. The force-extension data at low forces (<100 pN) were fit to a WLC model that included axial extension as described above. This corresponds to a bead displacement of < 100 nm (typical trap stiffness was ~1-2 pN nm^{-1}) where the linear approximation of the trap is reliable. The WLC model was then used to predict the force applied to the fibril at larger bead displacements where it behaves linearly. (Our position detector could accurately measure the position of the bead up to displacements of ~ 300 nm). Since the fibril force and the trap force are in equilibrium, the WLC predicted force is equivalent to the applied trap force. This analysis showed the trap could achieve 250 pN. Hence we used 250 pN as the maximum force capacity of our instrument.

Fitting the force-extension curves by a modified worm-like chain (WLC) model. Under no externally applied forces, NM fibrils exhibited end-to-end distances comparable to their fully extended length (contour length, L_c), indicating that L_p is of the same order at L_c. Therefore, the Palmer-Boyce WLC model, which is appropriate when $L_p \sim L_c$, was used to model the force-extension data [1]. Equations (1)-(3) were used to identify persistence length (L_p), contour length (L_C), and the axial stretching modulus (κ_A), from the force-extension data.

$$F = \frac{k_b T}{L_p}\left(\frac{1}{4\left(1-\lambda_u r_0 / L_C\right)^2}\right)\left(\frac{L_C / L_p - 6\left(1-\lambda_u r_0 / L_C\right)}{L_C / L_p - 2\left(1-\lambda_u r_0 / L_C\right)}\right) \qquad (1)$$

$$\lambda_e = \frac{L_C}{r_0}\frac{F}{\kappa_A} + 1 \qquad (2)$$

$$\lambda = \lambda_e \lambda_u = r / r_0 \qquad (3)$$

In these equations, F is the force acting on the fibril; λ is the total fibril stretch which is decomposed into λ_u, the stretch due to the reduction in thermal fluctuations of the fibril due to F, and λ_s, the stretch due to direct axial extension. r is the current end-to-end distance, and r_0 is the initial end-to-end distance, which is derived from equation (1) as $r_0 = L_C\left(1-\frac{L_C}{6L_p}\right)$. The data were fit in Matlab by minimizing the sum-squared error between the data and the WLC-predicted force. R^2 values were typically above 0.95. To fit the force-extension curves with discontinuities in the stretching phases, equations (1-3) were fit to force-extension data prior to unfolding. Then, L_C was adjusted in order to fit the data after unfolding. ΔL_C was determined by the L_C prior and after the discontinuities occurred.

When the histogram of fibril extension lengths (ΔL_C) obtained from unfolding at each force-dropping event was plotted, a well-established formula for determining optimal bin width for a histogram for a non-normal dataset was used [2]:

$$binwidth = \frac{2*(IQR)}{\sqrt[3]{\#observations}} \qquad (4)$$

where IQR is the interquartile range. As a result, 12nm band width was used for wild-type NM fibrils and 24nm was used for RΔ2-5.

Fitting the rupture lifetime of RΔ2-5 fibrils by a Bell model. The rupture events that occurred during the holding phase were fit to a Bell model [3] which describes the lifetime, τ, of a single interaction under an applied force, F.

$$\tau = \tau_0 \exp(-\beta F x^{\ddagger}) \qquad (5)$$

In this equation τ_0 is the bond lifetime under zero load, $x^{\ddagger}$ is the characteristic distance to achieve rupture, and β is $1/k_B T$. In our experiments, fibrils were comprised of several thousand monomers in series which all experience the load. The probability for a rupture event in the fibril is then the probability of rupture for a single interaction weighted by the total number of molecular interactions where rupture can occur (i.e. the number of monomers) assuming they are all mechanically similar. Alternatively, the lifetime of the amyloid fibril is inversely proportional to the number of monomers. To account for this increased probability of rupture in the fibril, the experimentally determined fibril lifetime was scaled by the number of monomers to identify an equivalent lifetime for a single monomer. The number of monomers in a fibril was

determined using a very rough estimate of 1.5nm/monomer (an approximate average of the two proposed structural models for NM fibrils) (*6-10*). Each fibril lifetime was scaled using its corresponding contour length to determine the number of monomers. The corrected data were then fit to equation (4) in Matlab by minimizing the sum-squared error between the natural log of equation (4) and the natural log of the data.

Movie S1. The NM fibrils were tethered to the glass surface. The movie was taken from a standard inverted fluorescence microscope with a 100x objective lens (field of observation 60 μm x 60 μm). The main bodies of the tethered fibrils were often out of focus as seen at the beginning of the movie. In the middle of the experiment, flow was introduced to straighten the fibrils for better visualization. The direction of the flow was changed during the experiments to demonstrate that these fibrils were indeed attached to the surface at one end while the main bodies were mobile.

Movie S2. Fluorescence image of tethered NM fibrils on the optical trapping instrument (field of observation 15 μm x 15 μm). The distribution of tethered fibrils in the movie was illustrated below. Fibrils with one end attached to the glass surface are highlighted by green arrows, while fibrils with both ends attached to the glass surface are highlighted by red arrows. We optimized the procedure for each experiment to reduce the number of fibrils double-tethered to the glass surface.

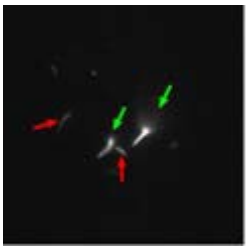

Movie S3. The NM prion domain from *Candida albicans* Sup35 homolog did not capture *S. cerevisiae* NM fibrils. When CaNM monomers were pre-deposited to the glass surface followed by casein blocking, ScNM fibrils were rarely recruited and tethered to the surface. Typically no more than three ScNM fibrils were observed in the field of observation (60 μm x 60 μm) and the movie showed the extreme.

Movie S4 – 6. Cleavage of NM monomers at the junction between the fibril and the glass surface released tethered NM fibrils.
S4. Before the TEV treatment to release tethered NM fibrils. The fluorescent channel was opened transiently for imaging to minimize fluorescence bleaching.
S5. After the TEV treatment to release tethered NM fibrils. 20 μl of 20 unit μl^{-1} TEV protease was introduced into the chamber by flow. This fluorescent image was recorded after 10-minute incubation of TEV protease. The bead that was previously attached to one end of the fibril and was trapped with the optical laser is visible in the image. However, the previously tethered fibril shown in movie S4 was no longer detected after the TEV protease treatment. We suspected that, after release from the glass surface, the flexible fibril might collapse and be hidden from view by the bead.
S6. After the TEV treatment to release tethered NM fibrils, imaged with a constant flow. To test if the released fibril was hidden from view by the bead, we asked if we could extend the hidden fibril with a constant flow of 1xCRBB buffer through the flow channel. The flow is readily

detectable in this movie by the free objects in the flow channel flowing from the left lower corner to the upper right corner in the movie. Indeed, in the presence of a constant flow, the fibril that had been released from the glass surface by the TEV cleavage was now visible, aligning itself with the flow.

Movie S7 - 8. Typical pulling behavior of tethered NM fibrils. Prior to each pulling experiment, the tethered fibril and the attached bead were fluorescently imaged to confirm the nature of the tethers. The instrument we employed to achieve low trapping forces allowed an interlaced optical force and fluorescence (IOFF). In short, fluorescence and excitation lasers were cycled out of phase at 50 kHz with a 10% duty cycle lag time in between to allow excited electrons to return to their ground state. This method prolonged the fluorescence signal from the bead and the fibril and enabled imaging of the fibril morphology throughout the force-extension experiment.
S7. Fluorescent image of the tethered NM fibril when the trapping laser was not turned on.
S8. The trapping laser was turned on to perform the pulling experiments.

Movie S9 - 14 . Direct observation of the rupture of tethered NM fibrils by fluorescent imaging. We trapped the bead at the extended position and manually aligned the fibril with the x-axis of the piezo stage without centering. Without the prolonged process of centering, trap-accelerated photo bleaching was minimized and fluorescent images could be recorded stably before rupture. Note however that the fragment of the fibril closest to the bead still became photobleached during this process. Constant high force was then applied to the bead in the absence of fluorescent imaging until the tether was ruptured. To establish the position of rupture, fluorescent imaging was re-initiated. In movies recorded after rupture, fragments of the previously tethered fibrils could be seen still attached to the surface, and these represented varying fractions of the initial fibril length. Other objects in the field of view provide a point of reference for the ruptured fibril.
S9 – 10. Rupture occurred in the middle of this fibril. S9, before rupture; S10, after rupture. The portion of the fibril left on the glass surface moved freely relative to the trapped bead after rupture. The trapped bead was able to move freely with pulling force, confirming that the connection to the fibril had been ruptured.
S11 – 12. Rupture occurred close to the bead. S11, before rupture; S12, after rupture.
S13 – 14. Rupture occurred close to the glass surface. S13, before rupture; S14, after rupture. The small fragment remaining on the surface couldn't be identified but the fibril, still attached to the bead, could be visualized. To ensure that rupture of the tether had occurred we then flowed buffer through the chamber. This reoriented the fibril – now tethered only to the bead – relative to its original orientation.

REFERENCES

1. Palmer, J.S. & Boyce, M.C. Constitutive modeling of the stress-strain behavior of F-actin filament networks. *Acta Biomater.* **4**, 597-612 (2008).
2. Izenman, A.J. Recent Developments in Nonparametric Density-Estimation. *J. Am. Stat. Assoc.* **86**, 205-224 (1991).
3. Bell, G.I. Models for Specific Adhesion of Cells to Cells. *Science* **200**, 618-627 (1978).
4. Bechtluft, P. et al. Direct observation of chaperone-induced changes in a protein folding pathway. *Science* **318**, 1458-1461 (2007).
5. Wang, H. et al. Direct and selective elimination of specific prions and amyloids by 4,5-dianilinophthalimide and analogs. *Proc. Natl. Acad. Sci. USA* **105**, 7159-7164 (2008).
6. Cao, Y. & Li, H. How do chemical denaturants affect the mechanical folding and unfolding of proteins? *J. Mol. Biol.* **375**, 316-324 (2008).